



HAL
open science

New insight into the aptamer conformation and aptamer/protein interaction by surface-enhanced Raman scattering and multivariate statistical analysis

Wafa Safar, Andra-Sorina Tatar, Aymeric Leray, Monica Potara, Qiqian Liu, Mathieu Edely, Nadia Djaker, Jolanda Spadavecchia, Weiling Fu, Sarra Gam Derouich, et al.

► To cite this version:

Wafa Safar, Andra-Sorina Tatar, Aymeric Leray, Monica Potara, Qiqian Liu, et al.. New insight into the aptamer conformation and aptamer/protein interaction by surface-enhanced Raman scattering and multivariate statistical analysis. *Nanoscale*, 2021, 13 (29), pp.12443-12453. 10.1039/D1NR02180J . hal-03369964

HAL Id: hal-03369964

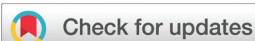
<https://hal.science/hal-03369964>

Submitted on 23 Nov 2021

HAL is a multi-disciplinary open access archive for the deposit and dissemination of scientific research documents, whether they are published or not. The documents may come from teaching and research institutions in France or abroad, or from public or private research centers.

L'archive ouverte pluridisciplinaire **HAL**, est destinée au dépôt et à la diffusion de documents scientifiques de niveau recherche, publiés ou non, émanant des établissements d'enseignement et de recherche français ou étrangers, des laboratoires publics ou privés.

COMMUNICATION

Cite this: *Nanoscale*, 2021, **13**, 12443

Received 7th April 2021,
Accepted 23rd June 2021
DOI: 10.1039/d1nr02180j
rsc.li/nanoscale

New insight into the aptamer conformation and aptamer/protein interaction by surface-enhanced Raman scattering and multivariate statistical analysis†

Wafa Safar,^a Andra-Sorina Tatar,^b Aymeric Leray,^c Monica Potara,^b Qiqian Liu,^d Mathieu Edely,^a Nadia Djaker,^d Jolanda Spadavecchia,^d Weiling Fu,^e Sarra Gam Derouich,^f Nordin Felidj,^f Simion Astilean,^b Eric Finot^c and Marc Lamy de la Chapelle^{*,a,e,g}

We study the interaction between one aptamer and its analyte (the MnSOD protein) by the combination of surface-enhanced Raman scattering and multivariate statistical analysis. We observe the aptamer structure and its evolution during the interaction under different experimental conditions (in air or in buffer). Through the spectral treatment by principal component analysis of a large set of SERS data, we were able to probe the aptamer conformations and orientations relative to the surface assuming that the in-plane nucleoside modes are selectively enhanced. We demonstrate that the aptamer orientation and thus its flexibility rely strongly on the presence of a spacer of 15 thymines and on the experimental conditions with the aptamer lying on the surface in air and standing in the buffer. We reveal for the first time that the interaction with MnSOD induces a large loss of flexibility and freezes the aptamer structure in a single conformation.

Introduction

Biosensors are designed to specifically detect analytes. The specificity is provided by multiple and simultaneous bio-

molecular recognition events based on weak interactions, which give apparent affinity. Aptamers are new bioreceptors intensively used now in biosensors. They are composed of a single DNA strand that offers many advantages such as high affinity *versus* analytes,¹ high stability and highly reproducible *in vitro* production with high purity excluding any use of animals or cells.^{2–4} Through the self-hybridisation of one part of its sequence, the aptamer forms a loop structure, exposing some bases that interact specifically with the analyte due to electrostatic interactions.

It is of primary importance to understand such interactions to optimize the analyte capture and to improve the sensing performances as one of the main drawbacks of biosensors is the biological noise due to unspecific interactions that constrain the detection limit.⁵ Indeed, as the bioreceptor can interact with molecules other than its specific target, non-specific binding can occur and induce a ‘biological noise floor’. Consequently, the analyte of interest cannot be detected below this biological noise. In addition, molecular interactions are the basis of many biological mechanisms. It is therefore important to have a better understanding of these phenomena and be able to answer the following specific questions: How does the interaction take place? Is it dynamic or static? Is there any specific conformation for the interaction?

Several techniques can give access to structural information on biomolecules such as NMR or IR absorption. However, to have enough signal/noise ratio, they need to study simultaneously a large number of molecules either in highly concentrated solutions or on large surfaces with high coverage rates. Thus, such techniques provide average information on the biomolecules and cannot observe the interaction at the individual level due to a lack of sensitivity or a limited spatial resolution. For instance, NMR needs a large quantity of materials⁶ (weight in the milligram range or concentrations in the millimolar range), whereas for IR absorption, the lateral spatial resolution

^aIMMM – UMR 6283 CNRS, Le Mans Université, Avenue Olivier Messiaen, 72085 Le Mans, Cedex 9, France. E-mail: marc.lamydelachapelle@univ-lemans.fr

^bBabes-Bolyai University, Institute for Interdisciplinary Research in Bio-Nanosciences and Faculty of Physics, Nanobiophotonics and Laser Microspectroscopy Center, 1 Str. M Kogalniceanu, RO-400084 Cluj-Napoca, Romania

^cLaboratoire Interdisciplinaire Carnot de Bourgogne, UMR 6303 CNRS, Université de Bourgogne Franche Comté, F-211078 Dijon, France

^dCNRS, UMR 7244, CSPBAT, Laboratoire de Chimie, Structures et Propriétés de Biomatériaux et d’Agents Thérapeutiques, Université Paris 13, Sorbonne Paris Cité, Bobigny, France

^eDepartment of Clinical Laboratory Medicine, Southwest Hospital, Third Military Medical University, Chongqing, China

^fUniversité de Paris, ITODYS, CNRS, UMR 7086, 15 rue J-A de Baïf, F-75013 Paris, France

^gSTAR Babes-Bolyai University Institute, 1 Str. M Kogalniceanu, RO-400084 Cluj-Napoca, Romania

† Electronic supplementary information (ESI) available. See DOI: 10.1039/d1nr02180j

(around 10 μm) is restricted by the diffraction limit in the IR wavelength range⁷ (2.5–25 μm).

To obtain a clear insight into the interaction, there is a need to observe a small quantity of molecules especially if the interaction is dynamic and the bioreceptor flexible. It can give rise to several configurations of the interaction through different structures or conformations.

Surface-enhanced Raman scattering (SERS) can overcome such limitations. As one vibrational spectroscopy technique and thanks to the huge Raman signal enhancement,⁸ SERS can probe the molecular structure and has paved the way to single-molecule sensitivity.^{9–11}

It has been demonstrated that SERS enables the observation and study of DNA strands¹² and the detection of medical targets for clinical applications.^{13,14} Indeed, the SERS spectrum is strongly related to the strand sequence and is sensitive to any sequence modification at the single base level.^{15–18} It also provides information on the interaction with a complementary strand (hybridisation),^{19,20} with exogenous agents²¹ or with the surface (strand orientation).^{22–24} Alternative complementary methods based on plasmonic devices were also proposed in the literature to study DNA or RNA strands in small quantities or even at the individual strand level. For instance, tip-enhanced Raman scattering (TERS) was used to identify the RNA strand sequence,²⁵ nanopores surrounded by plasmonic bullseye were used to observe DNA translocation under heating²⁶ or nanopipettes were designed as supports for SERS or TERS to detect individual molecules.²⁷

However, even if DNA strands were intensively studied by SERS, no study was specifically devoted to the aptamer structure and the influence of its interaction with the analyte on its conformation. As aptamers were used as bioreceptors in SERS sensors, their SERS spectrum is known and corresponds essentially to the ones obtained for DNA strands, including the contribution of the nucleosides contained in the sequence, and their interaction with the analytes was observed in a sensing objective.^{28–31} Spectral variations in the aptamer spectra were detected with an increase of the analyte concentration and interpreted as an increase of the number of interacting aptamers, but no interpretation of the aptamer structure during the interaction was provided.^{32,33} Moreover, no study of the aptamer alone was performed.

Understanding such an interaction is highly relevant as it was observed that for the same active sequence, the interaction depends strongly on the presence of a spacer or the grafting method when the aptamer is immobilised on a surface.^{34–36}

As the aptamer is a macromolecule made of a long chain of nucleosides, it is flexible³⁷ and could present different structural configurations when it is alone or when it is in interaction. To probe this complexity, one should screen the different configurations experienced by the aptamer under specific conditions and determine their effects on the aptamer structure.

To obtain a clear and relevant insight, we propose to combine the following two approaches: the mapping of a SERS

surface covered by aptamers and the statistical analysis of spectral data. The former allows us to measure the SERS spectra on a very large number of reduced areas (surface around 1 μm^2) containing a few aptamers. We should then be able to screen a sufficient number of situations related to all the potential structural conformations of the aptamers. In addition, the latter allows us to extract all the structural information and discriminate the different contributions present in the spectral data depending on the surface location.

Our methodology was applied to one aptamer specific to manganese superoxide dismutase (MnSOD), an oxidoreductase that induces the dismutation of superoxide anions in oxygen and hydrogen peroxide and is known to be a biomarker of some cancers.³⁸ We were able to observe different structures and orientations of the aptamer in relation to the SERS surface depending on its interaction with MnSOD. We interpret this structural and orientation dispersity as evidence for the flexibility of the aptamer under different experimental conditions (in air or in buffer) and of the structural constraints induced by the interaction.

Results and discussion

Two aptamers, Apt-wT and Apt-w/oT, were used. Both have the same active sequence for MnSOD capture, but in the Apt-wT, we included a sequence of 15 thymines at its 5' end to increase the distance of the active sequence from the gold surface. Both aptamers also include a thiol group at their 5' end to graft the aptamer on the gold nanoparticle surface (Fig. 1a).

The aptamers in the buffer solution (PBS buffer 10 \times : 1.37 M sodium chloride, 0.027 M potassium chloride, and 0.119 M phosphate buffer) are deposited on the surface of arrays of gold nanocylinders (Fig. 1b and c) whose geometrical parameters were optimised for the SERS measurements at 633 nm.^{8,39–41} After 12 h of incubation, the surface is washed

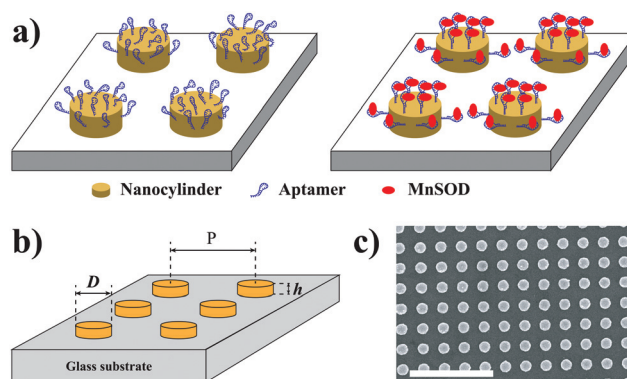


Fig. 1 (a) Principle of the SERS experiments. The gold nanocylinders are covered by aptamers alone (left) or interacting with MnSOD (right). (b) Scheme of the SERS substrate (P : array period, D : nanocylinder diameter and h : nanocylinder height). (c) SEM image of the nanocylinder array ($P = 340$ nm, $D = 140$ nm and $h = 50$ nm, scale bar: 1 μm).

with the buffer solution to remove all the aptamers not grafted on the nanocylinder surface and is dried.

SERS mapping including several tens of points (one or several maps of several tens of points with a step of $1\ \mu\text{m}$, a theoretical spatial resolution of $860\ \text{nm}$) is performed, and one SERS spectrum is recorded on each point. Such mappings were performed under different conditions: in air after surface drying and in the buffer solution. In this latter case, a drop of the buffer solution was deposited on the substrate. More than 350 spectra were recorded under the four conditions (see Experimental for more details).

The same procedure was applied to study the interaction of apt-wT with MnSOD in the buffer solution. Different concentrations of MnSOD (1 nM, 10 nM, 100 nM and 1000 nM) were deposited to observe the influence of the MnSOD interaction on the aptamer structure. This concentration range was chosen as the affinity constant for the aptamer *vs.* MnSOD and was calculated to be $330\ \text{nM}$.²⁸ Then, our experiments cross over this affinity constant and we could observe the interaction not only under low event conditions at low concentrations but also close to the saturation for the highest concentration.

All the spectral data (more than 700 spectra for all conditions and concentrations; the whole sets of spectra are shown in Fig. S1 and S2†) were analyzed by principal component analysis (PCA) to understand the wide spectral variations observed in the mapping. We obtained a sufficient number of data to extract relevant information on spectral variations to identify the key spectral components and determine the contribution of different bands in the spectral variations. Our objective is to determine whether the observed variations are simply related to intensity modification or to more complex variations depending on the experimental conditions (air or buffer), on the presence of the thymine spacer or on the interaction with MnSOD.

We first studied the two aptamers alone in air and in the buffer. The mean spectra for the four situations are shown in Fig. 2a and b. One can observe strong differences between Apt-wT and Apt-w/oT, whereas only an intensity decrease is observed between air and buffer conditions. For both aptamers, the Raman features can be assigned to the bands of the different bases that compose the DNA strand and to the P-O bands from the DNA backbone (see Table S1† for a detailed assignment; a comparison with the classical Raman spectrum can be found in ref. 33). The Apt-wT Raman spectra are dominated by the T band contributions (strong bands at 1370 and $1250\ \text{cm}^{-1}$), whereas the Apt-w/oT Raman spectra are dominated by the A and G bands (strong bands between 1400 and $1700\ \text{cm}^{-1}$) (Fig. 2). It is known that the Raman intensity strongly depends on the type of bases with the following distribution: $I_A \gg I_G > I_C \approx I_T$.²³ Thus, as the Apt-wT spectra are dominated by the T bands, we assume that the signal from the other bases is less enhanced and we observe the bases closest to the gold surface. This is in agreement with the enhanced field extension estimated to be around $10\ \text{nm}$ with lithographed nanostructures and with an exponential decrease at the power ten.⁴² Thus, we essentially observe the T spacer in

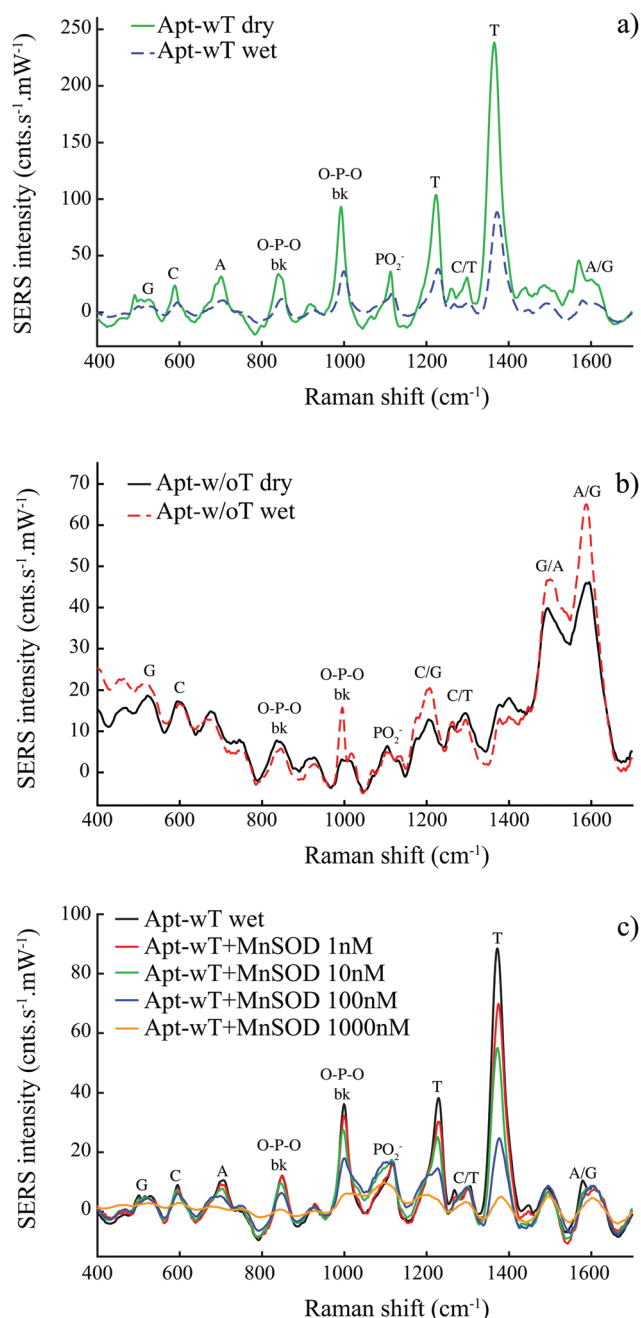


Fig. 2 (a) Average SERS spectra of the aptamer with the T spacer (apt-wT) recorded in air (green spectrum) or in the buffer (blue spectrum), (b) average SERS spectra of the aptamer without the T spacer (apt-w/oT) recorded in air (black spectrum) or in the buffer (red spectrum) and (c) average SERS spectra of the aptamer with the T spacer (apt-wT) recorded in the buffer for different concentrations of MnSOD (black spectrum: 0 nM, red spectrum: 1 nM, green spectrum: 10 nM, blue spectrum: 100 nM, orange spectrum: 1000 nM).

Apt-wT with a few contributions from P-O and the first bases of the active sequence. For Apt-w/oT, with the absence of the T spacer, we observe a mix of different contributions from the bases but dominated by the A and G bands as they are the most enhanced.

Some large signal variations are observed in SERS mapping in air or in the buffer. Such variations are too large to be simply due to enhancement fluctuation on the surface (reproducible SERS substrate with a small deviation of the signal) or due to the plasmon resonance shift (Fig. S3†). To have a better understanding of such signal modifications, we performed an analysis of the whole set of data including the Raman spectra obtained for the two aptamers in air and in the buffer. The results are presented in Fig. 3. Two main components can be extracted. Their contribution to the spectral features is very high as they represent more than 85% of the whole components (Fig. S4†) and highly relevant to the spectral variations. PC1 is dominated by the T and P-O bands, whereas PC2 is dominated by the A and G bands (Fig. 3a). The other components (PC3 and higher components) have limited contributions (less than 5%, as shown in Fig. S4†) and can then

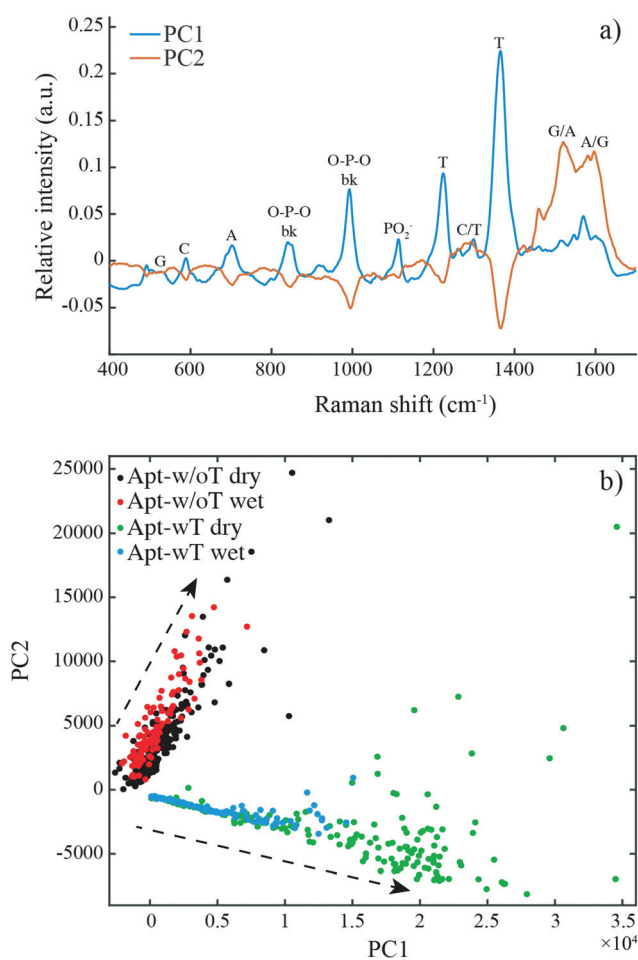


Fig. 3 (a) Principal components for the analysis of the aptamer with and without the T spacer in air and in the buffer (blue curve: PC1 and orange curve: PC2), (b) PC scores for the aptamer with and without the T spacer in air and in the buffer (black dots: aptamer without the T spacer in air, red dots: aptamer without the T spacer in the buffer, green dots: aptamer with the T spacer in air, blue dots: aptamer with the T spacer in the buffer). The dashed arrows indicate the aptamer orientations from “standing” to “lying” strands.

be neglected in the clustering analysis. In order to demonstrate this assumption, we represented the PCA analysis using the PC3 component in Fig. S5.† One can notice that the consideration of this component does not provide any further information or better clustering of the dots. Moreover, PC3 does not exhibit more bands or different features from PC1 and PC2 and thus does not provide further details on the spectral variations.

For Apt-wT in air or in the buffer (Fig. 3b), the dots are perfectly aligned at an angle of 15–20° from PC1 for small values of PC1 (below 10⁴) with a negligible contribution of PC2 and then start to diverge with a larger dispersion, especially in air (green dots). Thus, in the buffer, the SERS spectra are then largely dominated by the T bands, whereas in air, for a large contribution of the T bands, the green dots are more dispersed along PC2 (with even some positive values for PC2), indicating that the A and G contributions are no more negligible. Such intensity increase can be interpreted as a higher number of bases in the enhanced field and then as an aptamer closer to the gold surface.

Even if the dot distributions in air or in the buffer have similar behaviours, the dot spreading along PC1 largely decreases in the buffer, meaning that the buffer spectra experience much lower intensity variations than air ones and air spectra are much highly enhanced compared to buffer ones.

For apt-w/oT (Fig. 3b), the dots are nearly aligned accordingly to PC2, indicating a large contribution of the A and G bases with a limited contribution of the T bases, in accordance with the composition of apt-w/oT. The same conclusion as that for apt-wT can be pointed out: the dots are a little bit more spread out along the PC2 direction in the case of air relative to that in the buffer.

It is already demonstrated that for a negatively charged gold surface, the DNA strand interacts mainly through the nucleoside side and not through its backbone formed by the phosphate group.¹² Thus, the SERS spectra are dominated by the base features as effectively observed by a smaller intensity for P-O bands. Second, the SERS intensity is not only determined by the distance to the gold surface, meaning a higher signal for bases closer to the surface, but also by modified Raman selection rules as the enhanced vibration modes are those whose motions are perpendicular to the surface.⁴³ As the nucleosides are planar structures, their SERS intensity strongly depends on their orientation relative to the gold surface.²⁴ Thus, when the strand is parallel to the surface, the bases are perpendicular to the surface, exhibiting a large enhancement of their in-plane modes. Inversely, when the strand is perpendicular to the surface, the bases are parallel to the surface, inducing a strong decrease of the SERS signal of the in-plane modes. As the features observed in the SERS spectra of both Apt-wT and Apt-w/oT and PC1 and PC2 are assigned to in-plane modes, we could assume that SERS intensity variations are related to the DNA strand orientation (Fig. 2 and 3): an intensity increase is relevant to a strand more parallel to the surface (strand “lying” on the gold surface), whereas a decrease is relevant to a strand more perpendicular to the surface

(“standing” strand). Thus, the SERS intensity is a direct probe of the strand orientation and the statistical SERS variation is relevant to the orientation dispersity and heterogeneity on the gold surface.

Let us first focus on the Apt-wT alone. As already noticed, the dot dispersion is largely higher for the aptamer in air than in the buffer. Thus, in air, the aptamer is mostly “lying” on the surface, whereas it is more often “standing” in the buffer solution. The aptamer exhibits different behaviors in air and in the buffer as different kinds of interactions could occur inside the aptamer layer. Indeed, in air, the interactions are dominated by the van der Waals forces, whereas in the solution, the main forces are related to electrostatic repulsions through the Dujarguin–Landau–Verwey–Overbeek (DLVO) interactions. Under our experimental conditions, the distances between two strands in the monolayer can be estimated to be around 2 and 4 nm (for a strand size estimated between 25 and 30 nm).^{35,44,45} In air, the distances are too large for van der Waals interactions. The strands have then the possibility to lie on the surface, inducing a large SERS signal. On the contrary, in the buffer, the repulsive forces occur on larger distances and the strands should stand mostly perpendicular to the surface. Under both conditions, we observe a wide range of conformations from “standing” to “lying” strands with various distributions from buffer to air conditions (Fig. 4).

For Apt-w/oT, the dot distribution is more compact and is nearly identical between air and buffer. The conformations seem to be less dispersed and more fixed, with the strands having a similar orientation distribution in both cases. Apt-w/oT have fewer possibilities of orientation than Apt-wT. This reveals that Apt-w/oT can adopt a fewer number of conformations and is less flexible than Apt-wT. The T spacer should give larger flexibility to the aptamer and allow it to reach more conformations. Such observation is in agreement with other

studies concerning the incorporation of a spacer at the extremity of the aptamer. First, molecular dynamics calculations provide the following estimation of the length for different numbers of T bases in the spacer sequence: 3.2 nm for 6 T and 5.6 nm for 20 T.⁴⁶ In our case, we could estimate the spacer length to be around 4 nm. Thus, such a length is large enough to avoid interactions of the aptamer active sequence with the gold surface and provide higher flexibility to the aptamer. In this sense, such an increase of flexibility has an impact on the targeting ability of the aptamer. Thus, it was already proposed that the incorporation of a spacer, such as several thymine bases, at the extremity of the aptamer sequence maximises the efficiency of the aptamer targeting ability^{46–48} as it can render the active sequence more accessible to its analyte. For instance, it has been demonstrated that the incorporation of 12 T greatly improves the detection sensitivity (an increase of nearly 10 times).⁴⁷

After deposition of MnSOD on the SERS substrate, the mean apt-wT Raman spectra exhibit the same features with slight band broadening (Fig. 2c), but the SERS intensity of the features assigned to the T base and P–O continuously decreases when the concentration increases. As already noticed, the enhancement extension in SERS is limited to the first nanometers from the gold surface⁴² and the contribution of the analytes located at a distance higher than 3 nm is lower than one-tenth of the SERS spectrum. Thus, we can assume that when MnSOD is interacting with the aptamer, it is located at a distance higher than 3 nm, and as a consequence, the MnSOD contribution is negligible and not observable in the SERS spectrum. Moreover, the estimated distance between two aptamers is lower than 4 nm (see the Experimental section for more details). As MnSOD has a larger size (estimated to be around 5 nm), we can also assume that the steric hindrance does not allow it to have direct access to the gold surface and will not allow the observation of its SERS spectrum. This access to the gold surface could only be considered when MnSOD replaces the aptamer. However, this latter one is grafted on the gold surface through a S–Au bond that is largely stronger than the electrostatic interaction. The replacement of the aptamer by MnSOD would mean the breaking of such S–Au bond, which is highly unlikely. Then, a very few numbers of proteins could be directly in contact with the gold surface and not be observable in SERS.

Moreover, as shown in Fig. S3,† the deposition of MnSOD on the SERS substrate induces only a slight shift of the plasmon resonance (estimated to be around 10 nm for the highest MnSOD concentration). Such a shift cannot explain the large signal decrease. Indeed, as demonstrated in ref. 40, with such a kind of nanostructures (nanocylinders), a shift of the plasmon resonance of 10 nm will induce a decrease in the Raman signal of around 10% and no more than 20%.

We performed PCA of the whole set of data including the aptamer alone and all the MnSOD concentrations. The first component, PC1 (Fig. 5a), has a high weight since it represents more than 70% of the whole components (Fig. S4)†. It is dominated by the aptamer SERS spectra alone with main contri-

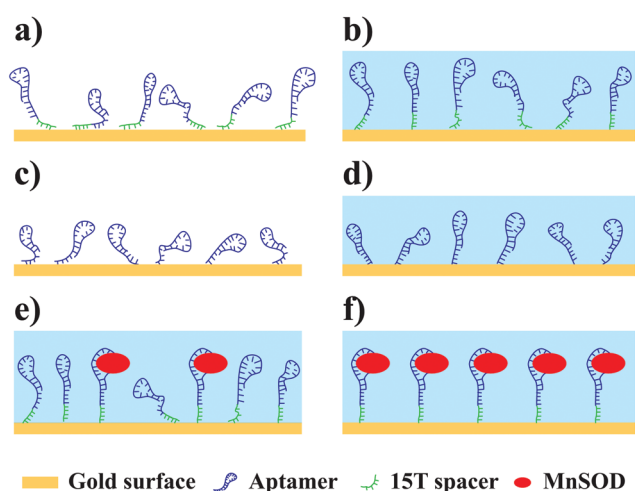


Fig. 4 (a–d) Schemes of the aptamer orientation for Apt-wT (a and b) and Apt-w/oT (c and d) alone in the buffer (a and c) and in air (b and d) and (e–f) schemes of the aptamer orientation for Apt-wT interacting with MnSOD at different concentrations (e: low concentration, f: high concentration).

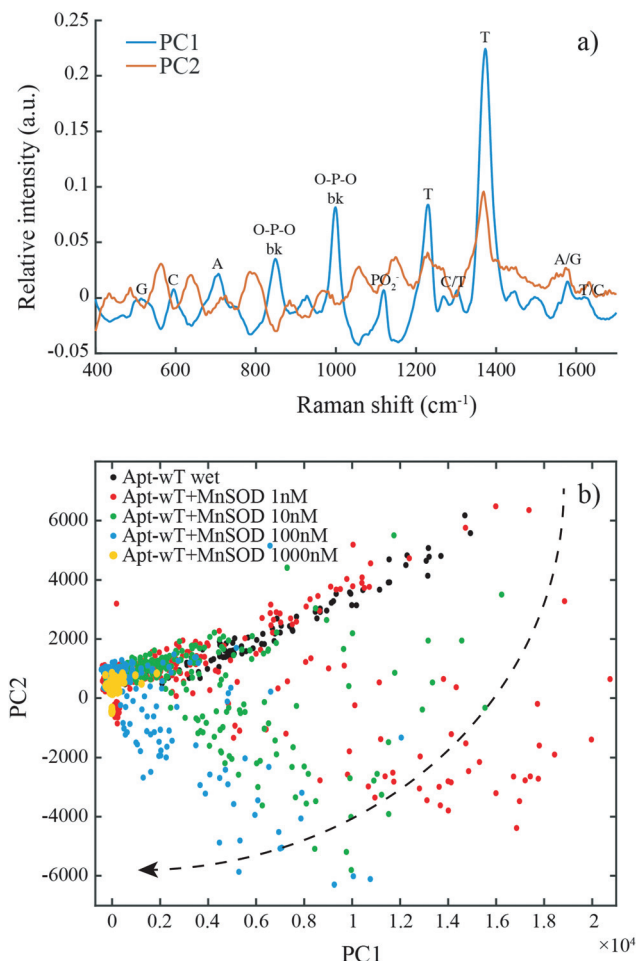


Fig. 5 (a) Principal components for the analysis of the aptamer with the T spacer in interaction with different concentrations of MnSOD (blue curve: PC1 and orange curve: PC2) and (b) PC scores for the aptamer with the T spacer in interaction with different concentrations of MnSOD (black dots: 0 nM, red dots: 1 nM, green dots: 10 nM, blue dots: 100 nM, yellow dots: 1000 nM). The dashed arrow indicates the aptamer orientations from “lying” to “standing” strands.

butions from T and P–O as previously described. PC2 does not exhibit specific features with a strong decrease of the bands assigned to the aptamer.

The distribution of the spectra is very wide between PC1 and PC2 (Fig. 5b), but one can observe a clear trend in the evolution of the dot distribution according to the MnSOD concentration. For the aptamer alone, the dots are nearly aligned with limited dispersion around the alignment, exhibiting a similar behavior than in the previous comparison with Apt-w/oT. At the opposite, for the largest MnSOD concentration, the dots are all concentrated in a small area with very low dispersion. For intermediate concentrations (from 1 to 100 nM), there is high dispersion of the dots. However, one can notice some evolution of the distribution when the concentration increases. For 1 nM, a large number of dots are aligned with the aptamer alone with a deviation of some dots. When the concentration increases, the dots are more and more deviated

from the aptamer alone with a decrease of the PC1 contribution and become closer to the PC2 axis. There is a tilting of the dots from PC1 to PC2. To explore this assumption, we calculated the angular dot distribution for the different concentrations (0° corresponding to PC1 axis and 90° to PC2 axis). To avoid any confusion, we represent the absolute values of the angles in Fig. 6a. We observe an increase of the median angle with the MnSOD concentrations from 20° for the aptamer alone to 90° for the largest MnSOD concentration with a fast variation around the affinity constant (330 nM).

We also observed much higher dot dispersion along PC2 for the 3 lowest concentrations (below the affinity constant) compared to the two extreme values (0 and 1000 nM) cor-

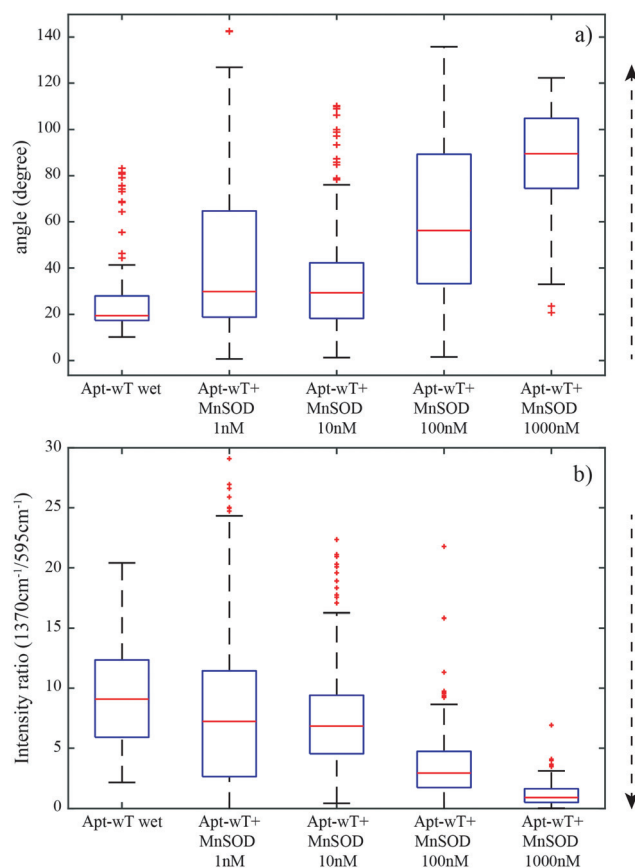


Fig. 6 (a) Angular dispersion of PCA dots for the aptamer with the T spacer in interaction with different concentrations of MnSOD (apt-wT wet: 0 nM, apt-wT wet + MnSOD 1 nM: 1 nM, apt-wT wet + MnSOD 10 nM: 10 nM, apt-wT wet + MnSOD 100 nM: 100 nM, apt-wT wet + MnSOD 1000 nM: 1000 nM) and (b) intensity ratio between the band at 1370 cm^{-1} and the band at 595 cm^{-1} for the aptamer with the T spacer in interaction with different concentrations of MnSOD (apt-wT wet: 0 nM, apt-wT wet + MnSOD 1 nM: 1 nM, apt-wT wet + MnSOD 10 nM: 10 nM, apt-wT wet + MnSOD 100 nM: 100 nM, apt-wT wet + MnSOD 1000 nM: 1000 nM). For each figure, the red line corresponds to the median (50% of the population), the blue box to the quartile deviation ($\pm 25\%$ of the population around the median), the black lines to 1.5 times the quartile deviation and the red dots to the outliers. For both figures, the dashed arrows indicate the aptamer orientations from “lying” to “standing” strands.

ponding to the lack of interaction or the saturation of the aptamer (Fig. 5b). Thus, PCA gives evidence for a continuous transition between the aptamer alone and the saturated situation that is directly related to the SERS intensity variation and more especially with the decreasing contribution of PC1 and the T bases to the SERS spectra.

Let us now explain such a result in the context of the orientation of the aptamer as determined previously and apply this assumption to the Apt-wT/MnSOD interaction. For the highest MnSOD concentration, the PC1 intensity and thus the T base contribution become very low, which means that the aptamer must have the preferential orientation perpendicular to the gold surface. Moreover, the dots are concentrated, meaning that there are few spectral variations and therefore few variations of the orientation. The aptamer loses its flexibility and freezes in a fixed conformation. The interaction with MnSOD selects a specific aptamer conformation and fixes it (Fig. 4f).

For the other concentrations, the dot dispersions indicate large heterogeneity of the aptamer conformations but with an evolution going from a highly flexible aptamer when alone to a frozen interacting aptamer. When MnSOD concentrations are lower than the affinity constant, the uptake rate of aptamers with the protein must be largely lower than 50% (1 and 10 nM) or close to but lower than 50% (100 nM). Some of the aptamers are therefore alone, while others are involved in the interaction.

As the affinity constant of MnSOD with the aptamer has been measured at 330 nM, the two concentrations of 100 nM and 1000 nM surround the affinity constant value, revealing two completely different behaviors. Indeed, at 1000 nM, the aptamer layer is saturated. In this situation, all the aptamers should have similar conformations with close structures and exhibit a nearly unique SERS spectrum, inducing reduced dispersion of the dots in PCA. On the contrary, at 100 nM (or for lower concentrations), less than 50% of the aptamers are interacting with one MnSOD molecule. This means that a large variety of aptamer conformations from the aptamer alone and the aptamer in interaction are observable, inducing a large variation of SERS signals and high dispersion of the dots in the PCA. Such reasons explain the large difference in the clustering behavior for these two concentrations.

The spectral and angular variations are therefore representative of the occupancy rate of the aptamers. We could determine the rate of aptamers interacting with MnSOD (occupation rate) using the median angle of each concentration (Table S2†). If we assume that the median angle of 20° corresponds to a rate of 0% (no MnSOD) and that the median angle of 90° corresponds to a rate of 100% (aptamer layer saturation), we find the occupation rates (Table S2†) close to what we could expect. The angular dispersion of the dots on the PCA provides a mapping of the aptamer/MnSOD interaction.

We can also propose a spectral probe to determine whether MnSOD is interacting with the aptamer. For this, we use the intensity ratio between two aptamer features: the 1370 cm⁻¹ band assigned to the T base, whose intensity strongly depends on the aptamer orientation (therefore on the interaction), and

the 595 cm⁻¹ band assigned to the cytosine cycle deformation. We choose this latter band as its intensity is nearly constant with the MnSOD concentration (Fig. S8†) even if it is weak, whereas the former one exhibits a large modification of its intensity with an increase of the MnSOD concentration (Fig. S8†). This ratio can then be used to monitor the evolution of the relative intensity of the 1370 cm⁻¹ band and can be relevant to the modification of the aptamer conformation during the interaction. A decrease of the I_{1370}/I_{595} ratio can be observed when the MnSOD concentration increases (Fig. 6b). The median value follows the Langmuir law reflecting the molecular interaction, whereas the dispersion of values indicates the interaction distribution. This latter can also be related to the high flexibility of the aptamer alone and the aptamer interacting with low concentrations of MnSOD (up to 10 nM). On the contrary, the interaction with a large amount of MnSOD (100 nM and 1000 nM) induces a reduction in the dispersion value and confirms the loss of flexibility and fixation of the aptamer in a specific and rigid conformation during the interaction.

Conclusions

In this paper, we exploited Raman spectroscopy to study the structure of aptamers alone and aptamers interacting with proteins and SERS to access a small number of molecules at the same time. SERS surface mapping allows the observation of large spectral variations that can be treated using PCA. We were able to correlate the spectral variations with the aptamer orientation relative to the gold surface. We demonstrated that the aptamer orientation depends on the experimental conditions (“standing” aptamer in the solution and “lying” aptamer in air). Such orientation variations also depend on the presence of a T spacer that provides higher flexibility to the aptamer.

During the interaction with MnSOD, the aptamer flexibility is highly reduced and the MnSOD interaction freezes the aptamer conformation. The aptamer is then a highly flexible molecule that can experience various conformations to recognise MnSOD, but the aptamer is blocked in a specific conformation to capture MnSOD. Our experience provides evidence for the dynamics of the aptamer/protein interaction that goes largely beyond the simple key/lock model. By mapping the interaction, we think that it will be possible to observe its spatial dispersion and the MnSOD surface coverage. Finally, the determination of spectral parameters allows us to identify the interaction and obtain a deep insight into the interaction mechanisms.

Experimental

Chemicals

The aptamer for MnSOD was purchased from Eurogentec and dispersed in PBS buffer (pH = 7.4). Manganese superoxide dis-

mutase (MnSOD) was purchased from Ab Frontier (LF-P0013, Superoxide Dismutase 2, Human, Euromedex).

Aptamers

The following two sequences were used for the aptamer:

5'HS-(C6)-TTTTTTTTTTTTTTTTT-CTTCTCTAGCTGAATAACCGGAAGTAACATCATCGTTTCGATGAGTTACTTCCGGTTATTCAGCTAGAGAAG 3'

and

5'HS-(C6)-CTTCTCTAGCTGAATAACCGGAAGTAACATCATCGTTTCGATGAGTTACTTCCGGTTATTCAGCTAGAGAAG 3'.

The first one is called Apt-wT, and the second one is Apt-w/oT.

The active sequence that captures MnSOD is composed of 71 bases from the first C at the 5' end to the last G at the 3' end. It forms a loop that will interact specifically with MnSOD. The aptamer was designed by the SELEX method in order to define the active sequence that has the highest affinity for MnSOD. More details can be found in ref. 28. The affinity of this aptamer toward MnSOD was measured by a quartz crystal microbalance (QCM) at 330 nM, as already published in ref. 28. In Apt-wT, a spacer of 15 thymines is included at the 5' end to increase the distance of the active part of the aptamer from the gold surface.

Based on the dynamics calculations done on different numbers of T bases in the spacer sequence,⁴⁶ we estimate the spacer length to be around 4 nm. Such a length is large enough to avoid interactions of the aptamer active sequence with the gold surface but is small enough to keep the aptamer in the enhanced field to provide the SERS signal. 15 T was then chosen to get a good compromise between these two parameters.

To graft the aptamer onto the gold surface, a thiol group was also included at the 5' end to form a S–Au bond and immobilise the aptamer on the SERS active surface.

Nanostructures

For the SERS measurements, we used some arrays of nanocylinders (Fig. 1) produced by electron beam lithography on glass substrate covered with a thin film of ITO (80 nm). The nanocylinders have a diameter, D , of 140 nm and a height, h , of 50 nm. The array period, P , is fixed to 340 nm in both directions to have a gap between the nanocylinders of 200 nm in order to avoid any short-range coupling.

Deposition of aptamers and MnSOD on the nanocylinder surface

The aptamers and the MnSOD proteins are dissolved in 10× PBS buffer (1.37 M sodium chloride, 0.027 M potassium chloride, and 0.119 M phosphate buffer) with a pH of 7.4. This neutral pH was chosen to avoid any influence of the pH on the interaction process. Indeed, if the pH is changed, the polarity of the solution will also change, inducing potentially a modification of the electrostatic interactions between the aptamers and consequently a modification of their structure or the distance between them on the gold surface.

The aptamer concentration is fixed at 100 μ M. For MnSOD, four solutions are prepared with the following concentrations: 1 nM, 10 nM, 100 nM and 1000 nM.

For each molecule and concentration, 10 μ l of solution is deposited on the nanocylinder surface. The surface is incubated for 12 h and then rinsed with distilled water to remove all the molecules not interacting with the surface. If any ungrafted aptamers are still present on the nanocylinder surface, they should be much less in number than the grafted aptamers. Indeed, as the ungrafted molecules are bonded to the gold surface with weak interactions, we expect that washing flux will remove a large majority of the ungrafted aptamers. Thus, their contribution, if any, should be negligible in the SERS signal.

The aptamer is first grafted on the surface and MnSOD is deposited in an increasing concentration. The effectiveness of aptamer grafting and MnSOD deposition and its interaction with the aptamer was monitored by the shift of the plasmon resonance measured at each step of the process (Fig. S3†).

Plasmon resonance measurement

The plasmon resonance was measured using an Xplora Raman spectrophotometer (Horiba Scientific). The nanostructures are illuminated by a halogen lamp located below the SERS substrate, and the transmitted light is collected using a 10× microscope objective with a low numerical aperture (0.25) to avoid the collection of the scattered light. A reference spectrum is recorded without the nanostructures (only the glass substrate). The plasmon resonance is then calculated by dividing the transmitted spectrum of the nanostructure with the reference spectrum to remove the lamp contribution and the optical transfer function of the spectrometer.

SERS mapping

SERS mapping is performed using an Xplora Raman spectrophotometer (Horiba Scientific) equipped with an Olympus microscope. We used a HeNe laser (638 nm, 1.4 mW) and a 100× microscope objective (numerical aperture = 0.9) to reach a theoretical spatial resolution of 860 nm. The spectral resolution is 2 cm^{-1} . For each molecule and concentration, we recorded several tens of points on the SERS surface by performing one or several maps of several tens of points with a step of 1 μ m (the exact number of points is given in S1 and S2†). We did not perform exactly the same number of points to have a random distribution of the studied aptamers alone or in interaction. The accumulation time was adapted to each condition in order to get an exploitable signal/noise ratio (Apt-wT in air: 5 s, Apt-wT in buffer: 45 s, Apt-w/oT in air: 15 s, Apt-w/oT in buffer: 30 s, Apt-wT + 1 nM of MnSOD: 40 s, Apt-wT + 10 nM of MnSOD: 40 s, Apt-wT + 100 nM of MnSOD: 40 s, Apt-wT + 1000 nM of MnSOD: 60 s).

For one spot, we excite a limited number of nanocylinders (between 6 and 7). Each nanocylinder has a whole surface of 37 400 nm^2 . From previous studies performed under similar conditions, the coverage rate of a single DNA strand monolayer was determined to be in the range between 3.7×10^{13} strands

per cm^2 and 6×10^{12} strands per cm^2 for DNA strands deposited on gold flat surface^{35,44,45} or on colloidal nanoparticles,³⁵ which corresponds to a distance between two strands in a 2D square-packed monolayer of around 2 and 4 nm, respectively. If we take an average distance of 2.8 nm between 2 aptamers, we probed around 4800 aptamers per nanocylinder and thus around 31 000 aptamers per spot. These numbers are the upper limit as the whole nanocylinder surface is not SERS active or a large part of the surface has a limited contribution to the SERS signal.⁴⁹ One can then assume that in one spot we probe effectively a few thousands of aptamers. On a whole map of 100 spots, it makes few hundreds of thousands of aptamers probed, which gives access to large distribution and a relevant insight into the aptamer conformations and allows a statistical analysis of the data.

The mappings in air were performed directly on the dry surface. For the measurement in the buffer solution, a drop of buffer (10 μl) was deposited on the substrate and a glass slice (thickness of 180 μm) was deposited above to avoid the evaporation of the solution, forming a thin film of around 100 μm in thickness. This latter thickness (t) is estimated using the volume of the buffer ($V = 10 \mu\text{l}$) deposited on the substrate surface and the approximative size of the drop formed on the substrate surface ($S \approx 1 \text{ cm}^2$) after the coverage by the glass slice. In this case, the thickness is calculated as $t = V/S \approx 100 \mu\text{m}$.

Before principal component analysis, the baseline of all the Raman spectra was corrected using the automatic function of LabSpec 6 software (Xplora Raman spectrophotometer, Horiba Scientific). During the PCA treatment, all the spectral data were normalised compared to the accumulation time and laser power.

The excitation laser polarisation was linear and parallel to the substrate surface. We assume that this parameter has little influence on our SERS measurements because the aptamers are grafted onto the whole surface of the nanocylinders (on top and edges) and it is therefore not possible to define a clear polarisation direction with respect to the orientation of the aptamers. The aptamers are therefore considered to be randomly distributed with respect to the polarisation of the excitation laser. In the discussion, we have therefore only considered the orientation of the aptamers with respect to the surface of the nanocylinder and not with respect to the laser polarisation direction.

The reference Raman spectrum of the buffer was also recorded under similar conditions (accumulation time: 130 s, laser power: 16 mW) and is shown in Fig. S7.† As no signal of the buffer can be recorded in the solution, the buffer has been dried on the substrate and the signal was recorded on a crystal formed on the substrate surface.

Principal component analysis (PCA)

PCA is a well-established multivariate analysis technique that reduces the dimensionality of a matrix of data to few principal components, which can be visualized graphically, with minimal loss of information. In this representation, the new variables also called principal components are uncorrelated

and they correspond to a linear combination of the original ones. Computationally, PCA consists of finding the eigenvalues and eigenvectors (also called PC scores and PC loadings, respectively) of the covariance matrix. Before calculating the covariance matrix, experimental SERS spectra were first corrected in order to take into account the fact that the exposition time, the laser intensity and the Raman shift range were not constant between each experimental series. These corrected spectra were then centered, signifying that the mean of each spectrum was subtracted. The PC loadings and PC scores of each corrected spectrum were resolved by using a homemade program written in MATLAB (version R2018a, The MathWorks). The PC scores of the first and second PC loadings were finally plotted. In this representation, each point corresponds to one corrected SERS spectrum.

We have represented in Fig. S1 and S2† the whole sets of baseline-corrected SERS spectra recorded with the aptamers alone (Apt-wT and Apt-w/oT) in air and in the buffer and with Apt-wT in the buffer interacting with different concentrations of MnSOD. The main visible variations are due to intensity fluctuations that can be explained by the fact that the enhancement factor is not exactly identical when the laser is focused on different positions of the SERS substrate. These variations of SERS spectra are also visible in PCA representation with the presence of a branch that has already been attributed to enhancement factor variations.⁵⁰

Author contributions

WS, AT, MP and LQ performed the experiments and interpreted the data. AL and EF interpreted the data by PCA. SR and NF produced the SERS substrates. ME, AL, EF and MC conceived the experiments. WS, ME, AL, EF, ND, JS, WF, NF, SA and MC analysed the data and wrote the manuscript.

Conflicts of interest

There are no conflicts to declare.

Acknowledgements

This work is supported by the Louise project (ANR-15-CE04-0001) and the Nanobiosensor project (ANR-15-CE29-0026) from the French National Research Agency (ANR). Members of IMMM acknowledge support from the Région Pays de la Loire (France, Pari scientifique X-TREM project) and the National Natural Science Foundation of China (no. 81920108024). Members of ICB acknowledges support from the Bourgogne Franche-Comté Graduate School EUR-EIPHI (17-EURE-0002), the Région Bourgogne Franche Comté (PARI II NANO2BIO and contract CIME), and the European Union (FEDER-FSE Bourgogne 2014-2020). Marc Lamy de la Chapelle acknowledges the STAR Babes-Bolyai University Institute for financial support.

References

- 1 L. Gold, B. Polisky, O. Uhlenbeck and M. Yarus, *Annu. Rev. Biochem.*, 1995, **64**, 763–797.
- 2 S. Tombelli, M. Minunni and M. Mascini, *Biosens. Bioelectron.*, 2004, **20**, 2424–2434.
- 3 S. D. Jayasena, *Clin. Chem.*, 1999, **45**, 1628–1650.
- 4 T. Mairal, V. C. özalp, P. L. Sánchez, M. Mir, I. Katakis and C. K. O'Sullivan, *Anal. Bioanal. Chem.*, 2008, **390**, 989–1007.
- 5 J. L. Arlett, E. B. Myers and M. L. Roukes, *Nat. Nanotechnol.*, 2011, **6**, 203–2015.
- 6 A.-H. M. Emwas, R. M. Salek, J. L. Griffin and J. Merzaban, NMR-Based Metabolomics in Human Disease Diagnosis: Applications, Limitations, and Recommendations, *Metabolomics*, 2013, **9**, 1048–1072.
- 7 P. Lasch and D. Naumann, Spatial Resolution in Infrared Microspectroscopic Imaging of Tissues, *Biochim. Biophys. Acta, Biomembr.*, 2006, **1758**, 814–829.
- 8 N. Guillot and M. L. de la Chapelle, *J. Quant. Spectrosc. Radiat. Transfer*, 2012, **113**, 2321–2333.
- 9 S. Nie and S. R. Emory, *Science*, 1997, **275**, 1102–1106.
- 10 K. Kneipp, Y. Wang, H. Kneipp, L. T. Perelman, I. Itzkan and R. R. Dasari, *Phys. Rev. Lett.*, 1997, **78**, 1667–1670.
- 11 E. C. Le Ru, E. Blackie, M. Meyer and P. G. Etchegoin, *J. Phys. Chem. C*, 2007, **111**, 13794–13803.
- 12 E. Garcia-Rico, R. A. Alvarez-Puebla and L. Guerrini, *Chem. Soc. Rev.*, 2018, **47**, 4909–4923.
- 13 S. Laing, K. Gracie and K. Faulds, *Chem. Soc. Rev.*, 2016, **45**, 1901–1918.
- 14 M. Green, F. M. Liu, L. Cohen, P. Köllensperger and T. Cass, *Faraday Discuss.*, 2006, **132**, 269–280.
- 15 L. J. Xu, Z. C. Lui, J. Li, C. Zong, C. J. Yang and B. Ren, *J. Am. Chem. Soc.*, 2015, **137**, 5140–5154.
- 16 J. Morla-Folch, H. Xie, P. Gisbert-Quilis, S. Gomez de Pedro, N. Pazos-Perez, R. A. Alvarez-Puebla and L. Guerrini, *Angew. Chem., Int. Ed.*, 2015, **54**, 13650–13654.
- 17 J. Morla-Folch, P. Gisbert-Quilis, M. Masetti, E. Garcia-Rio, R. A. Alvarez-Puebla and L. Guerrini, *Angew. Chem., Int. Ed.*, 2017, **56**, 2381–2385.
- 18 E. Papadopolou and S. E. J. Bell, *Angew. Chem., Int. Ed.*, 2011, **50**, 9058–9061.
- 19 L. Guerrini, Ž. Krpetić, D. van Lierop, R. A. Alvarez-Puebla and D. Graham, *Angew. Chem., Int. Ed.*, 2015, **54**, 1144–1148.
- 20 A. Barhoumi, D. Zhang, F. Tam and N. J. Halas, *J. Am. Chem. Soc.*, 2008, **130**, 5523–5529.
- 21 M. Masetti, H. N. Xie, Z. Krpetic, M. Recanatini, R. A. Alvarez-Puebla and L. Guerrini, *J. Am. Chem. Soc.*, 2015, **137**, 469–476.
- 22 E. Papadopolou and S. E. J. Bell, *Chem. Commun.*, 2011, **47**, 10966–10968.
- 23 A. Torres-Nuñez, K. Faulds, D. Graham, R. A. Alvarez-Puebla and L. Guerrini, *Analyst*, 2016, **141**, 5170–5180.
- 24 L. He, M. Langlet, P. Bouvier, C. Calers, C. M. Pradier and V. Stambouli, *J. Phys. Chem. C*, 2014, **118**, 25658–25670.
- 25 E. Bailo and V. Deckert, Tip-enhanced Raman Spectroscopy of Single RNA Strands: Towards a Novel Direct-sequencing Method, *Angew. Chem., Int. Ed.*, 2008, **47**, 1658–1661.
- 26 C. R. Crick, P. Albella, H.-J. Kim, A. P. Ivanov, K.-B. Kim, S. A. Maier and J. B. Edel, Low-Noise Plasmonic Nanopore Biosensors for Single Molecule Detection at Elevated Temperatures, *ACS Photonics*, 2017, **4**, 2835–2842.
- 27 K. J. Freedman, C. R. Crick, P. Albella, A. Barik, A. P. Ivanov, S. A. Maier, S.-H. Oh and J. B. Edel, On-Demand Surface- and Tip-Enhanced Raman Spectroscopy Using Dielectrophoretic Trapping and Nanopore Sensing, *ACS Photonics*, 2016, **3**, 1036–1044.
- 28 M. Cottat, C. D'Andrea, R. Yasukuni, N. Malashikhina, R. Grinyte, N. Lidgi-Guigui, B. Fazio, A. Sutton, O. Oudar, N. Charnaux, V. Pavlov, A. Toma, E. Di Fabrizio, P. G. Gucciardi and M. L. de la Chapelle, *J. Phys. Chem. C*, 2015, **119**, 15532–15540.
- 29 C. V. Pagba, S. M. Lane, H. Cho and S. Wachsmann-Hogiu, *J. Biomed. Opt.*, 2010, **15**, 047006.
- 30 H. X. Wang, Y. W. Zhao, Z. Li, B. S. Liu and D. Zhang, *Sensors*, 2019, **19**, 3806.
- 31 B. C. Galarreta, M. Tabatabaei, V. Guieu and E. Peyrin, *Anal. Bioanal. Chem.*, 2013, **405**, 1613–1621.
- 32 G. R. Gillibert, M. N. Triba and M. L. de la Chapelle, *Analyst*, 2018, **143**, 339–345.
- 33 R. Yasukuni, R. Gillibert, M. N. Triba, R. Grinyte, V. Pavlov and M. de la C. Lamy, *Nanophotonics*, 2019, **8**, 1477–1483.
- 34 B. Waybrant, T. R. Pearce and E. Kokkoli, *Langmuir*, 2014, **30**, 7465–7474.
- 35 L. M. Demers, C. A. Mirkin, R. C. Mucic, R. A. Reynolds, R. L. Letsinger, R. Elghanian and G. Viswanadham, *Anal. Chem.*, 2000, **72**, 5535–5541.
- 36 C. Arib, Q. Liu, N. Djaker, W. Fu and M. L. de la Chapelle, *Plasmonics*, 2019, **14**, 1029–1038.
- 37 D. Y. Petrovykh, V. Perez-Dieste, A. Opdahl, H. Kimura-Suda, J. M. Sullivan, M. J. Tarlov, F. J. Himpsel and L. J. Whitman, *J. Am. Chem. Soc.*, 2006, **128**, 2–3.
- 38 A. Borrelli, A. Schiattarella, P. Bonelli, F. M. Tuccillo, F. M. Buonaguro and A. Mancini, *Biomed. Res. Int.*, 2014, **2014**, 1–11.
- 39 J. Grand, M. L. de la Chapelle, J.-L. Bijeon, P.-M. Adam, A. Vial and P. Royer, *Phys. Rev. B: Condens. Matter Mater. Phys.*, 2005, **72**, 033407.
- 40 F. J. Colas, M. Cottat, R. Gillibert, N. Guillot, N. Djaker, N. Lidgi-Guigui, T. Toury, D. Barchiesi, A. Toma, E. Di Fabrizio, P. G. Gucciardi, M. Lamy de la Chapelle, F. J. Colas, M. Cottat, R. Gillibert, N. Guillot, N. Djaker, N. Lidgi-Guigui, T. Toury, D. Barchiesi, A. Toma, E. Di Fabrizio, P. G. Gucciardi and M. L. de la Chapelle, *J. Phys. Chem. C*, 2016, **120**, 13675–13683.
- 41 N. Félidj, J. Aubard, G. Lévi, J. R. Krenn, A. Hohenau, G. Schide, A. Leitner and F. R. Aussenegg, *Appl. Phys. Lett.*, 2003, **82**, 3095.
- 42 J. A. Dieringer, A. D. McFarland, N. C. Shah, D. A. Sturat, A. V. Whitney, C. R. Yonzon, M. A. Young, X. Zhang and R. P. Van Duyne, *Faraday Discuss.*, 2006, **132**, 9–26.

- 43 M. Moskovits, D. P. DiLella and K. J. Maynard, *Langmuir*, 1988, **4**, 67–76.
- 44 D. Y. Petrovykh, H. Kimura-Suda, L. J. Whitman and M. J. Tarlov, *J. Am. Chem. Soc.*, 2003, **125**, 5219–5226.
- 45 R. Levicky, T. M. Herne, M. J. Tarlov and S. K. Satija, *J. Am. Chem. Soc.*, 1998, **120**, 9787–9792.
- 46 H. Xing, J. Li, W. Xu, K. Hwang, P. Wu, Q. Yin, Z. Li, J. Cheng and Y. Lu, *ChemBioChem*, 2016, **17**, 1111–1117.
- 47 Y.-H. Lao, K. Peck and L.-C. Chen, *Anal. Chem.*, 2009, **81**, 1747–1754.
- 48 E. Southern, K. Mir and M. Shchepinov, *Nat. Genet.*, 1999, **21**, 5–9.
- 49 R. Gillibert, M. Sarkar, J. Moreau, M. Besbes, M. Canva and M. L. de la Chapelle, *J. Phys. Chem. C*, 2016, **120**, 27562.
- 50 A. Leray, T. Brulé, M. Buret, G. Colas Des Francs, A. Bouhelier, A. Dereux and E. Finot, *Sci. Rep.*, 2016, **6**, 20383.